Composites Part B 194 (2020) 108034

Contents lists available at ScienceDirect

Composites Part B

journal homepage: www.elsevier.com/locate/compositesb

4D printed electro-induced continuous carbon fiber reinforced shape memory polymer composites with excellent bending resistance

Chengjun Zeng [a], Liwu Liu [a], Wenfeng Bian [b], Yanju Liu [a], Jinsong Leng [c,*]

[a] Department of Astronautical Science and Mechanics, Harbin Institute of Technology (HIT), No. 92 West Dazhi Street, PO Box 301, Harbin, 150001, People's Republic of China
[b] Department of Civil Engineering, Harbin Institute of Technology (HIT), Weihai, 264209, People's Republic of China
[c] National Key Laboratory of Science and Technology on Advanced Composite in Special Environments, Harbin Institute of Technology (HIT), Harbin, 150080, People's Republic of China

ARTICLE INFO

Keywords:
4D printing
Continuous carbon fiber
Shape memory polymer composites
Bending strength/modulus
Electro-induced

ABSTRACT

Four-dimensional (4D) printing technology of continuous carbon fiber reinforced shape memory polymer composites is a potential manufacturing process for lightweight and high-strength intelligent composite structures. In this study, a 3D printer with dual feed channels based on the fused deposition modeling (FDM) was designed to fabricate continuous carbon fiber reinforced shape memory poly(lactic acid)-based composites (CFRSMPC). The impact of various printing parameters on the bending strength and flexural modulus of 4D printed CFRSMPC was evaluated by the three-point bending test. Meanwhile, mathematical prediction models of bending strength and modulus based on the existing experimental data were established. The electro-induced shape memory effect of 4D printed CFRSMPC was investigated by the electric heating shape recovery test. The shape recovery rate of the specimens was more than 95%, indicating that the resistance heating method is stable and feasible. The quantitative effect of bending angle and temperature on the resistance of CFRSMPC during the programming and recovery process was further investigated. The results demonstrated that the real-time deformation of the CFRSMPC could be monitored by the resistance measurement method. It can be concluded that the CFRSMPC fabricated using the 4D printing method can serve as potential building blocks for electrically activated and deployable structures.

1. Introduction

Three-dimensional (3D) printing, also known as additive manufacturing (AM), can produce geometrically complex and highly personalized structures on demand [1,2]. This advanced manufacturing method is gradually becoming one of the core technologies of the manufacturing industry [3]. However, the structures prepared by 3D printing lack flexibility and environmental adaptability, impeding the application of 3D printed components in practical engineering structures [4,5]. In 2013, the Self-Assembly Lab of the Massachusetts Institute of Technology introduced the concept of 4D printing through PolyJet 3D-printing to fabricate smart materials [6]. The so-called 4D printing refers to a next-generation additive manufacturing technology that is applied to manufacture active materials with the capability to be programmably activated and transformed the configuration over time under an environmental stimuli [7–11].

Shape memory polymers (SMPs) are active materials commonly applied in 4D printed actuators and reconfigurable structures [12,13]. SMPs can fix a programmed shape and recover to a permanent shape in response to external stimuli such as heat [14], light [15], electric current [16], magnetic field [17], and others. Thermoplastic SMPs possess the advantages of low cost and printability but generally poor mechanical properties [18]. So far, the mechanical properties of 4D printed thermoplastic SMPs have been improved mainly by following two methods: one is to combine SMPs with elastic materials such as silicon elastomer [11,19] and spring sheet [18] for the improvement in the stored elastic strain energy of the printed composites; the other is to enhance the elastic modulus and strength of SMPs by doping reinforcing fillers like carbon nanomaterials [19,20], Fe_3O_4 nanoparticles [21,22] and chopped fibers [23]. Although the approach of combining elastic materials with SMPs can effectively improve the mechanical performance and recovery force of 4D printed structures, the non-integrated

* Corresponding author.
E-mail address: lengjs@hit.edu.cn (J. Leng).

https://doi.org/10.1016/j.compositesb.2020.108034
Received 23 December 2019; Received in revised form 30 March 2020; Accepted 1 April 2020
Available online 8 April 2020
1359-8368/

manufacturing process makes it difficult for SMPs and elastic materials to achieve synergistic deformation. On the other hand, particle fillers and chopped fibers make limited improvement in the mechanical properties of 4D printed SMPs.

The emergence of 3D printing process for continuous fiber reinforced thermoplastic composites provides new development opportunities for 4D printed active materials with competitive mechanical properties. The process embeds continuous fibers in the component by the integrated in-situ impregnation and fiber tension based on fused deposition modeling (FDM) [24,25]. Continuous carbon fiber (CF), often as reinforcing phase for advanced composites, possesses unique characteristics including excellent mechanical performance, flexible microstructure designability, and considerable electrical conductivity. Even though there are some investigations about the development and characterization of 3D printed continuous carbon fiber reinforced thermoplastic composites [26–28], these studies generally only use continuous carbon fibers as the mechanically enhanced phase of 3D printed structures without considering them as the reinforcing phase as well as heating elements of 4D printed active materials.

In this paper, continuous carbon fiber reinforced shape memory polylactic acid (PLA) composites (CFRSMPC) with prominent bending resistance was fabricated by exploiting a modified single nozzle 3D printer based on FDM. The coupling effects of various printing parameters such as extruder temperature, extrusion width, printing speed, and fiber infill angle on the bending properties of 4D printed CFRSMPC were evaluated to obtain optimized printing parameters. Furthermore, based on generalized printing parameters, the electrothermal drive characteristics and shape memory behavior of 4D printed CFRSMPC were investigated. A phenomenological model based on the macroscopic buckling of CF and the microscopic conductivity principle of graphite crystal lattice was proposed to explain the mechanism of electrical resistance change of the CFRSMPC during electrical activation. The results demonstrated that resistance measurement could serve as a novel approach to regulating the deployable configuration of 4D printed CFRSMPC.

2. Experimental section

2.1. Equipment and materials

The equipment involved in this study to fabricate continuous CF reinforced polymer composites was a modified single-nozzle 3D printer based on FDM technology. The printer before the modification was developed by Shenzhen Creality 3D Technology Co., Ltd., China. The main improvement was the addition of a CF feed channel on the extruder to enable the 3D printer to perform multimaterial 4D printing tasks. Fig. 1 is a schematic of the operation of the modified extruder from which it is observed that soft material and continuous CFs enter the extruder from two feed channels, respectively, and then the two phases are mixed and extruded from a single nozzle. The flexible consumables employed for 4D printed CFRSMPC were semi-crystalline PLA filaments with outstanding shape memory performance prepared by the research group of Professor Jinsong Leng [11,29]. The thermal properties of the PLA filaments were thoroughly investigated by differential scanning calorimetry (DSC) and thermal gravimetric analysis (TGA) [11]. The crystallization temperature and melting temperature of the filament are approximately 110 °C and 170 °C, respectively. The continuous CF tow was T300B-1000-50B produced by Toray Co., Ltd., Japan, which was composed of 1000 individual CF filaments, each having a diameter of 7 μm and electric resistivity of 1.7 × 10-3 Ω cm.

2.2. Specimen fabrication

The mechanical performance of 3D printed components based on FDM technology depends on the selection of structural parameters and process parameters [30]. In this study, the impact of four main

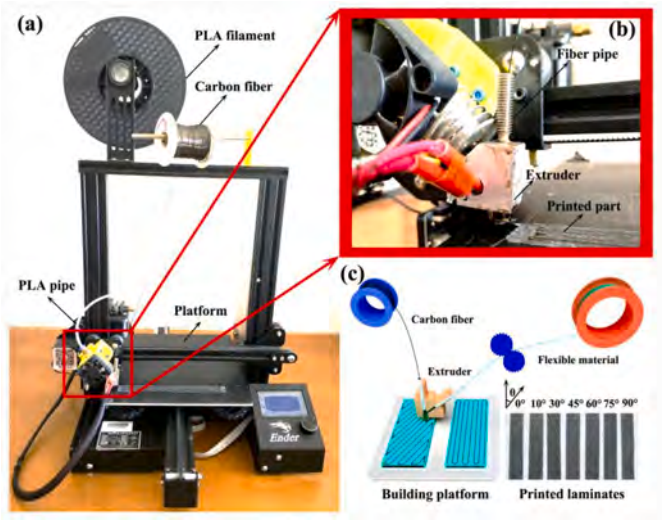

Fig. 1. Schematic of fabricating continuous carbon fiber reinforced polymer composites with a modified multi-material 3D printer based on FDM technology.

parameters such as extruder temperature (T), printing speed (S), fiber extrusion width (W), and fiber infill angle (θ) on the bending resistance of the printed CFRSMPC was investigated. The six various fiber extrusion width and fiber infill angle shown in Fig. 2 were considered as the main structural parameters, while the six different extruder temperature (180, 190, 200, 210, 220, and 230 °C) and printing speed (1, 2, 3, 4, 5, and 6 mm/s) were investigated as process parameters. Some printed specimens with different fiber infill angles are presented in the lower right corner of Fig. 1. According to the ASTM D790-07 standard, the geometrical dimensions of the specimens for the three-point bending test were determined to be 50.8 mm × 13.8 mm, with two layers of laid fibers and thickness of about 1.35 mm. In this study, the dynamic mechanical analysis (DMA) of printed composite specimens was carried out in accordance with the ASTM D4065-06 standard, and the dimension of the specimens used for DMA tests was 60 mm × 12 mm × 1.35 mm. Further, since there was no standard test method to determine the shape memory performance of 4D printed CFRP part, the size of the sample for shape recovery test was configured on being the same as that of the three-point bending test sample. In the valid range of printing parameters, the intermediate value is obviously more representative than other values. Hence, the extruder temperature, printing speed and fiber extrusion width of the specimens for the DMA and shape memory performance tests were determined to be 210 °C, 3 mm/s and 1.5 mm, respectively. Differently, the fiber infill angle was determined to be 0° to ensure the uniform distribution of the resistance of the specimen in the axial direction to facilitate electric heating.

2.3. Three-point bending test

Three-point bending tests were performed to characterize the bending resistance of 4D printed CFRSMPC. The testing equipment was a universal tester (Zwick Z010) from the Zwick/Roell Corporation. The tests were conducted with a span of 25.4 mm and a loading rate of 2.0 mm/min, and displacement-load curves were generated. Since support span-to depth ratios of the specimens during the tests is more than 16, according to ASTM D790-07, the stress in the outer surface of the sample can be reasonably approximated by the following equation.

$$\sigma_f = \frac{3PL}{2bd^2}\left[1 + 6\left(\frac{D}{L}\right)^2 - 4\left(\frac{d}{L}\right)\left(\frac{D}{L}\right)\right] \quad (1)$$

Where σ_f is the stress in the outer surface at the midpoint of the specimen, P is the load at a given point on the load-deflection curve, L is the

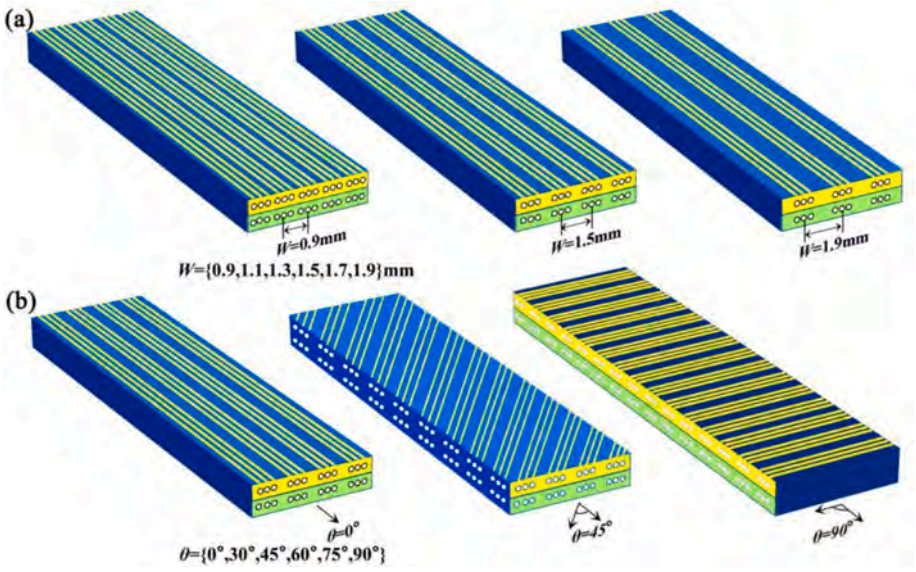

Fig. 2. Structural parameters of 4D printed CFRSMPC. a) Various fiber extrusion width. b) Various fiber infill angle.

support span, b is the width of the specimen, d is the thickness of the specimen, and D is the deflection of the centerline of the specimen at the midpoint of the span. In addition, flexural modulus E_f and the bending strain can be expressed by equations (2) and (3), respectively:

$$E_f = \frac{L^3 m}{4bd^3} \tag{2}$$

$$\varepsilon_f = \frac{6Dd}{L^2} \tag{3}$$

Where m is the slope of the initial straight-line segment of the load-deflection curve.

2.4. Dynamic mechanical analysis (DMA)

Storage modulus and glass transition temperature (T_g) are the key thermodynamic parameters associated with the shape memory effect of shape memory polymers, which should be measured for subsequent evaluation of the electro-induced shape memory behavior of 4D printed CFRSMPC. Moreover, it is necessary to characterize the impact of fiber incorporation on the storage modulus and T_g of the semi-crystalline PLA used. Therefore, a dynamic thermo-mechanical analyzer (TA Instrument DMA Q800) was used here to perform dynamic thermomechanical analysis on 4D printed pure PLA and CFRSMPC specimens. The tests were carried out in a double cantilever mode with a temperature sweep of 2 °C/min and a frequency of 1 Hz over a temperature range of 25 °C–100 °C.

2.5. Electric heating shape recovery test

4D printed specimens with conventional printing parameters were used to investigate the electro-induced shape memory effect of 4D printed CFRSMPC. In order to apply voltage to the sample conveniently, the conductive silver pulp was coated on both ends of the sample as the electrodes. Fig. 3a showcases a printed sample with silver coating at both ends. The CFRSMPC samples were deformed to a v-shape using three-point bending grips, which were mounted on a Zwick Z010 universal machine equipped with an environmental chamber, see Fig. 3b. This setup was used to fix the samples in their temporary shape at 90 °C using the environmental chamber, and then cooling to RT while keeping the samples under load. The electro-induced shape memory effect of 4D printed CFRSMPC was characterized by resistive heating. The shape recovery behavior was recorded by a video camera, and was quantified by the parameters such as recovery time t and bending angle α. Besides, an infrared thermal camera (VarioCAM HiRessl, JENOPTIK Infra Tec.) was used to monitor the transient temperature distribution of the specimens during resistance heating.

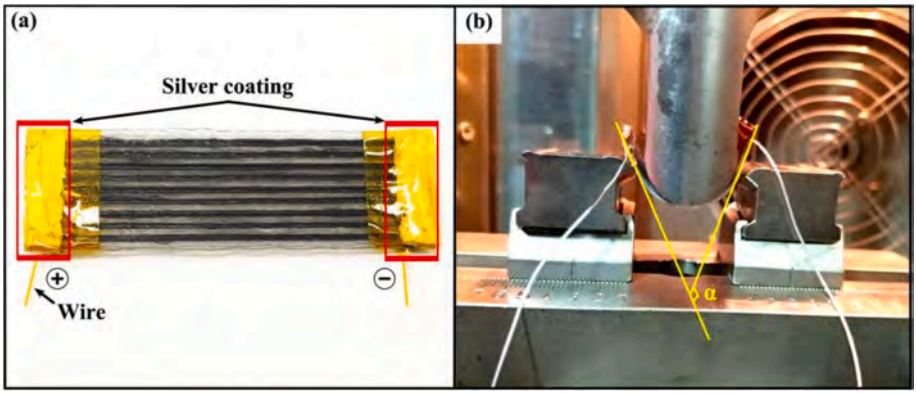

Fig. 3. a) 4D printed CFRSMPC specimen with silver coating on both ends as electrodes. b) Temporary shape and deformation angle of the specimen after being shaped.

2.6. Morphology characterization

The surface topography of CFRSMPC parts manufactured by FDM was observed using a VHX-900 super depth of field digital microscope (Keyence Co., Ltd., Osaka, Japan). The surface roughness *Ra* was calculated at four different positions for which average values were obtained, and three specimens were measured under each condition. After the three-point bending test, the microstructures of the fractured surfaces were observed by VEGA3 TESCAN scanning electron microscopy (SEM).

3. Results and discussion

3.1. Bending performance with printing parameter

3.1.1. Extruder temperature T

Temperature is one of the critical conditions for the preparation of carbon fiber reinforced polymer composites (CFRP) by 3D printing technology, which affects the impregnation of fibers and substrate. Fig. 4a shows a schematic of the displacement-load curves generated during the three-point bending test of specimens prepared under different extruder temperatures. It can be seen from the graph that the load response of the specimen fabricated at 180 °C is significantly lower than that of the specimens fabricated under higher temperature conditions when the same displacement occurs, indicating poor mechanical performance. PLA is a semi-crystalline polymer, and therefore the temperature for the 3D printing process based on FDM depends on its melting temperature. The melting temperature of the PLA-based SMP filament involved in this study is about 170 °C. When the extruder temperature is set to 180 °C, although the temperature in the liquefier has reached the melting temperature of the PLA-based SMP, the flowability of the melted PLA is still poor, and the impregnation between the molten matrix and the CFs is insufficient, resulting in the weak mechanical performance of the printed composite parts.

A more intuitive illustration of the effect of extruder temperature on the bending strength and flexural modulus of 4D printed CFRSMPC samples is presented in Fig. 4b. The bending properties are approximately positively related to the extruder temperature *T* from the 180 °C–230 °C. The bending strength and flexural modulus increase from 97.5 MPa to 3111 MPa–164.9 MPa and 4439 MPa, respectively. Through careful observation, it can be found that the bending strength and flexural modulus rise rapidly in the temperature range of 180 °C–200 °C. Conversely, from 200 °C to 230 °C, the bending strength and flexural modulus only experience a slight increase or even decrease at some specific temperature points. This phenomenon indicates that when the extruder temperature reaches about 200 °C, the melting degree of the PLA in the liquefier has already met the requirement for manufacturing composite members with excellent mechanical properties. Meanwhile, the elevated temperature may cause more serious thermal oxidation degradation of the matrix, resulting in the deterioration of mechanical properties [31], which can serve as an explanation for the degradation of bending strength and flexural modulus at some high temperature points. Compared with the pure PLA specimens fabricated by FDM process, the bending strength of the latter is about 52.6 MPa–57.9 MPa within the printing temperature range of 200 °C–230 °C [32], 4D printed CFRSMPC possesses prominently improved bending strength.

Fig. 5a and b exhibit the surface topography of the printed samples at the extruder temperatures of 230 °C and 180 °C, respectively, which can illustrate the surface quality of the parts. The surface roughness *Ra* of the CFRSMPC specimen printed with a temperature of 230 °C is 11.1 μm, which is smaller than the roughness of the sample printed at a temperature of 180 °C. The surface roughness data of CFRSMPC fabricated with various extruder temperatures presented in Supplementary material section S1 also indicates that the higher the extruder temperature is, the lower the surface roughness of 4D printed CFRSMPC components is. Similarly, Jaekel et al. [33] and Wang et al. [34] reported that higher temperatures provided more energy and allowed additional heating time for PEEK to crystallize, and increased crystallinity enhanced the elastic modulus and yield strength of PEEK while conferring lower surface roughness.

3.1.2. Printing speed S

Fig. 6 showcases the variation in displacement-load relationships, bending strength and flexural modulus of 4D printed CFRSMPC specimens manufactured using various printing speeds. The increased printing speed has a different degree of unfavorable influence on the bending strength and flexural modulus of the printed samples. When the printing speed is increased from 1 mm/s to 6 mm/s, the flexural modulus of the printed samples decreases significantly, which may be caused by the weak bonding strength between the fiber and the matrix as a result of the insufficient melting of the matrix. Moreover, as the printing speed increases, the increased flow rate of the molten matrix can cause a lower inner pressure in the liquefier, which also results in a decrease in the degree of impregnation of the matrix with the fibers.

It is anticipated that inadequate pre-impregnation between matrix and fibers and reduced pressure will also weaken the fiber/matrix bonding at the interface. This hypothesis can be confirmed by observing the fracture micromorphology of the samples manufactured at different printing speeds shown in Fig. 7. More fibers pull-out is observed at the fracture surface of the specimen manufactured with a printing speed of 6 mm/s (Fig. 7b) than the sample printed with a speed of 1 mm/s (Fig. 7a). The pull-out of fibers from PLA causes PLA to break first, and therefore the load cannot transfer to the fiber bundles, which results in a low flexural modulus of 2759 MPa (Fig. 6b). It can be seen from Fig. 6a and b that the bending strength of the printed sample is less affected by the printing speed. This observation is consistent with previous research results [35,36]. In fact, the strength of unidirectional fiber reinforced polymer composites is primarily dependent on the reinforced fibers, while the printing speed affects mostly the bonding between the fibers

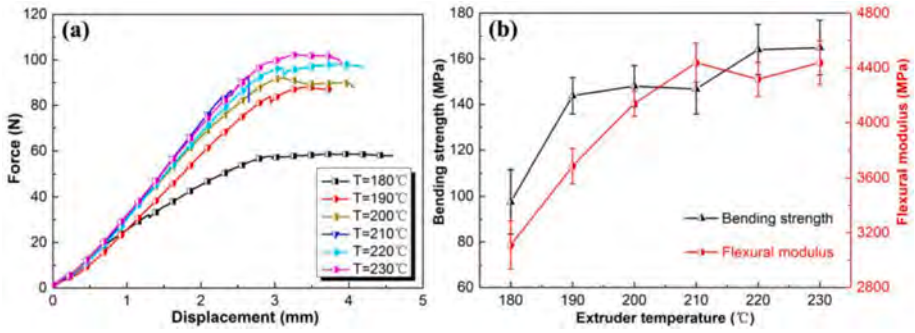

Fig. 4. Under the experimental conditions of $S = 3$ mm/s, $W = 1.5$ mm and $\theta = 0°$: a) displacement-load curves of 4D printed CFRSMPC specimens fabricated at various extruder temperatures; b) the effect of extruder temperature on the bending strength and flexural modulus of the printed CFRSMPC.

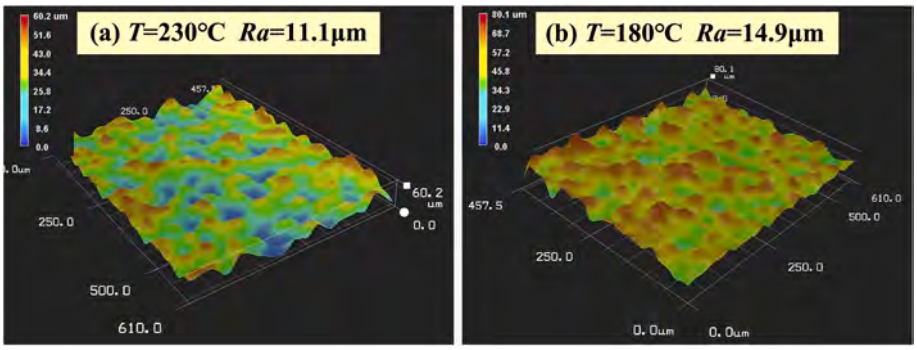

Fig. 5. Surface topography of the printed specimens fabricated at the extruder temperature of a) 230 °C and b) 180 °C, respectively.

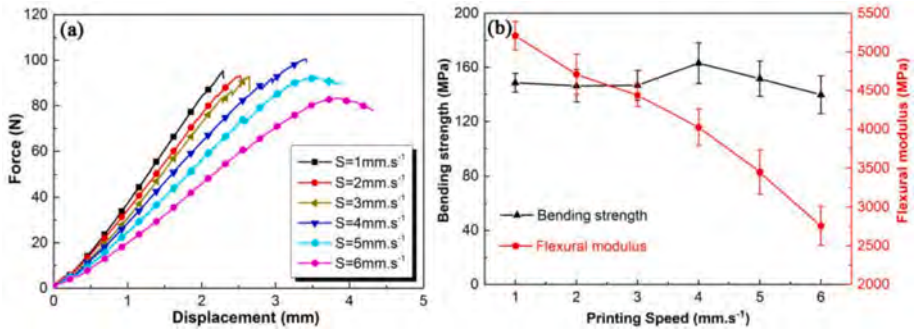

Fig. 6. Under the experimental conditions of $T = 210$ °C, $W = 1.5$ mm and $\theta = 0°$: a) Displacement-load curves of 4D printed CFRSMPC specimens fabricated at various printing speed. b) The effect of printing speed on the bending strength and flexural modulus of the printed CFRSMPC.

and the matrix. Fig. 8a and b show an increase in the mean surface roughness of the printed samples when the printing speed is increased from 1 mm/s to 6 mm/s, indicating that the surface roughness of 4D printed CFRSMPC parts is sensitive to the printing speed. When the printing speed is higher, the temperature of the PLA extruded by the nozzle drops at a faster rate, leading to less time for the diffusion and crystallization of the PLA molecular chain, which will increase the surface defects of the printed specimen.

3.1.3. *Extrusion width W and infill angle θ*

The displacement-load curves, bending strength, and flexural modulus of 4D printed CFRSMPC samples are exhibited in Fig. 9a and b as the functions of extrusion width *W*. As shown in Fig. 2a, extrusion width *W* is the central distance between two adjacent deposition lines extruded by the nozzle. The extrusion width directly identifies the volume fraction of CFs in the printed CFRSMPC. As shown in Fig. 9b, when the extrusion width is increased from 0.9 mm to 1.9 mm, the volume content of the fiber in the printed sample is reduced from 6.19 to 2.89%, by 53.3%. While the average bending strength and flexural modulus decrease from 212.4 MPa to 7397 MPa–77.3 MPa and 2534 MPa, with a reduction of 63.6% and 65.7%, respectively.

Mechanical properties are the outward manifestation of the microscopic fracture pattern. Fig. 10 exhibits the microscopic fracture pattern after the three-point bending test of 4D printed CFRSMPC samples manufactured at various extrusion width. When bending failure occurred for the sample printed with an extrusion width of 1.9 mm, brittle fracture of the matrix is observed from Fig. 10a, while the fiber bundles are pulled out without breaking, indicating that the fibers exert little reinforcement due to poor bonding between the fibers and the matrix. Fig. 10b displays the failure mode in which the fiber bundles and the matrix are almost neatly broken when the flexural failure of the sample fabricated at an extrusion width of 0.9 mm occurs, indicating good bonding between the fibers and the matrix. In general, small extrusion width improves the overlapping extent and achieves large contact pressure [35]. When extrusion width is reduced from 1.9 mm to 0.9 mm, the increased contact pressure motivates more molten PLA to be impregnated into the fiber bundles, improving the adhesion between the fibers and the matrix, and thus enhances the mechanical performance of the printed composite parts.

Whether the fiber layup angle is configurable is an important indicator for evaluating advanced composite manufacturing processes. The additive manufacturing process of continuous carbon fiber reinforced composites proposed in this study meets the requirements of the designability of fiber ply angle in advanced composite fabrication process, and laminates with different fiber infill angles have been prepared, as shown in Fig. 1c. Fig. 9c introduces the displacement-load curves of the printed samples with different fiber infill angles. It is noted that the mechanical response of the samples is highly sensitive to the fiber infill angle. The sample fabricated with infill angle of 0° has the maximum bending strength and flexural modulus, and does not substantially undergo a plastic yielding stage before bending failure, but the fracture strain is small. The samples printed with other fiber infill angles, especially when the infill angle is 45°, undergo a significant plastic deformation stage before failure. According to the experimental results, the fiber layup angle during the printing process can be designed to meet the requirements of the actual engineering for the mechanical properties of the printed components.

3.1.4. *Multivariable regression analysis*

The mathematical prediction models based on existing experimental data were developed to describe the coupling effect of printing parameters on the bending properties of 4D printed CFRSMPC. In this study, the multivariable quadratic regression model employed can be expressed via Eq. (4) [37].

$$Y = a_0 + \sum_{i=1}^{n} a_i x_i + \sum_{i=1}^{n} a_{ii} x_i^2 + \sum_{i<j}^{n} a_{ij} x_i x_j \tag{4}$$

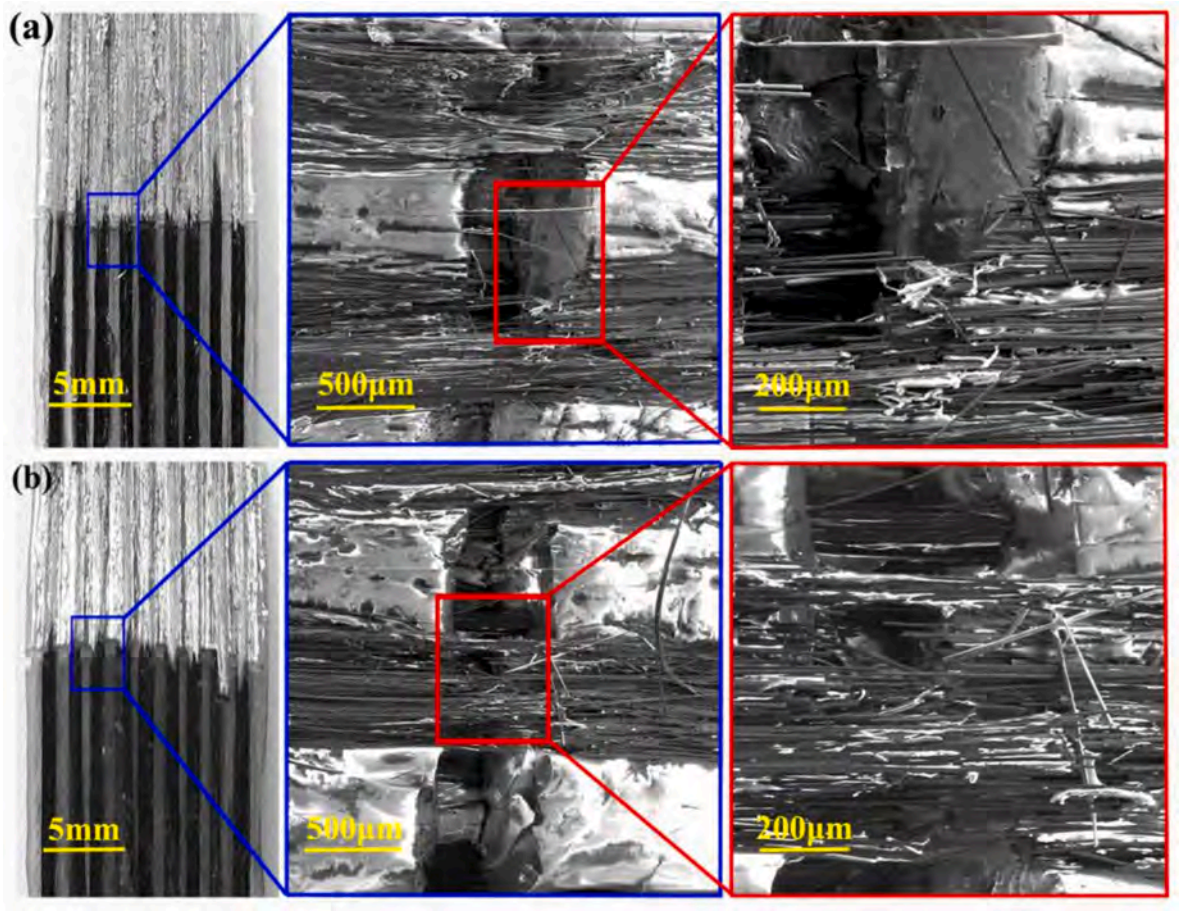

Fig. 7. Micromorphology of fracture surface after three-point bending test of the printed specimens with printing speed of a) 1 mm/s and b) 6 mm/s.

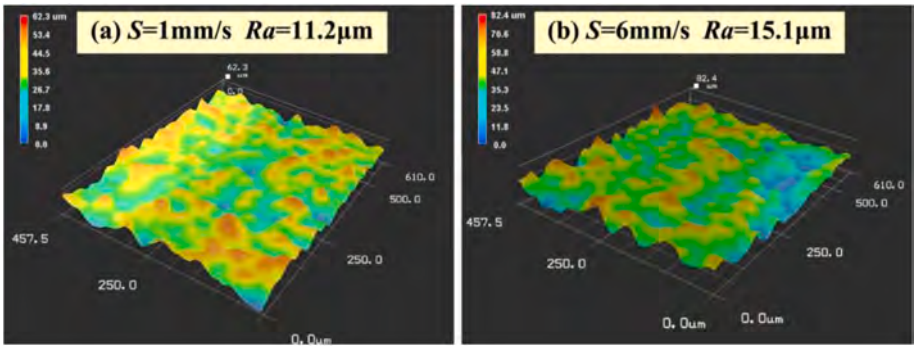

Fig. 8. Surface topography of the printed specimens fabricated at the printing speed of a) 1 mm/s and b) 6 mm/s, respectively.

Where Y represents the fitted response variable; x_i and x_j are independent variables; a_0, a_i, a_{ii}, and a_{ij} are coefficients for each term, and n is the total number of independent variables. Design Expert software was used to analyze the relationship between the bending responses (i.e., bending strength Σ_f and flexural modulus E_f) and the printing parameters (i.e., extruder temperature T, printing speed S, extrusion width W and infill angle θ) to obtain the regression coefficients. The accuracy of the prediction model was determined by the analysis of variance (ANOVA) method, in which the p-value and the coefficient of determination R-squared were observed. The input experimental data was presented in Supplementary material section S2. The obtained fitting results are as follows.

$$\sum_f = 102.6 + 1.937 \times T - 8.638 \times S - 155.4 \times W - 0.9034 \times \theta - 0.00079 \times T^2 + 8.024 \times S^2$$
$$+48.075 \times W^2 - 0.0058 \times \theta^2 - 0.1212 \times T \times S - 0.3123 \times T \times W + 0.0034 \times T \times \theta$$
$$-20.848 \times S \times W + 0.6243 \times S \times \theta - 1.475 \times W \times \theta, \quad (p - Value < 0.0001, R^2 = 96.4\%) \tag{5}$$

$$E_f = 6991.8 + 32.709 \times T - 415.33 \times S - 4903.9 \times W \quad - 28.454 \times \theta \quad - 0.09214 \times T^2 + 55.001 \times S^2$$
$$+206.70 \times W^2 - 0.07235 \times \theta^2 + 5.2996 \times T \times S + 9.5936 \times T \times W - 0.10375 \times T \times \theta$$
$$-980.63 \times S \times W + 11.829 \times S \times \theta - 8.3416 \times W \times \theta, (\ p - Value < 0.0001, R^2 = 97.6\%) \tag{6}$$

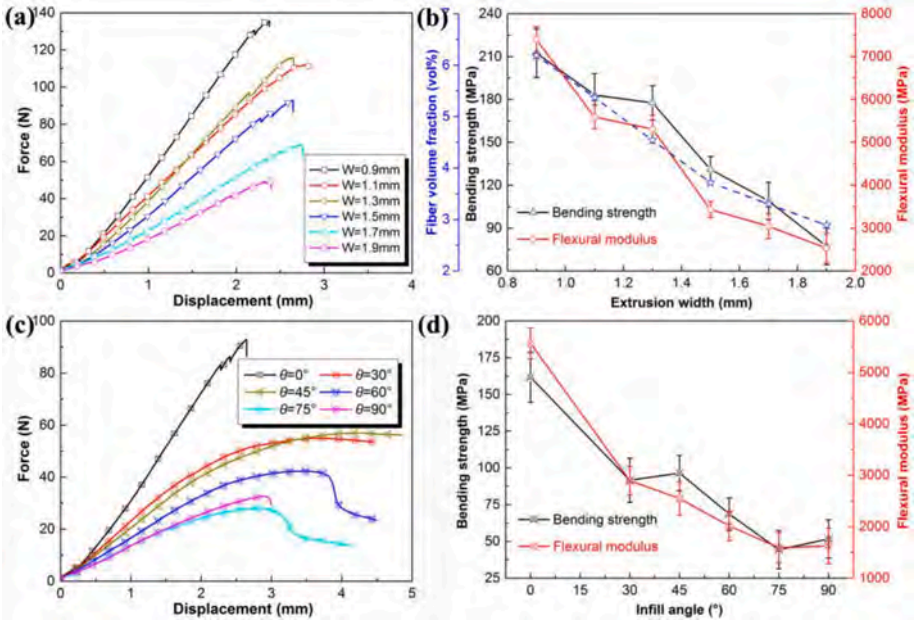

Fig. 9. The variation in a) displacement-load curves,b) flexural modulus and bending strength of the specimens printed with various extrusion width under other experimental conditions of $T = 210$ °C, $S = 3$ mm/s and $\theta = 0°$. c) Displacement-load curve, d) flexural modulus and bending strength of the printed specimens with different extrusion widths under other experimental conditions such as $T = 210$ °C, $S = 3$ mm/s and $W = 1.5$ mm.

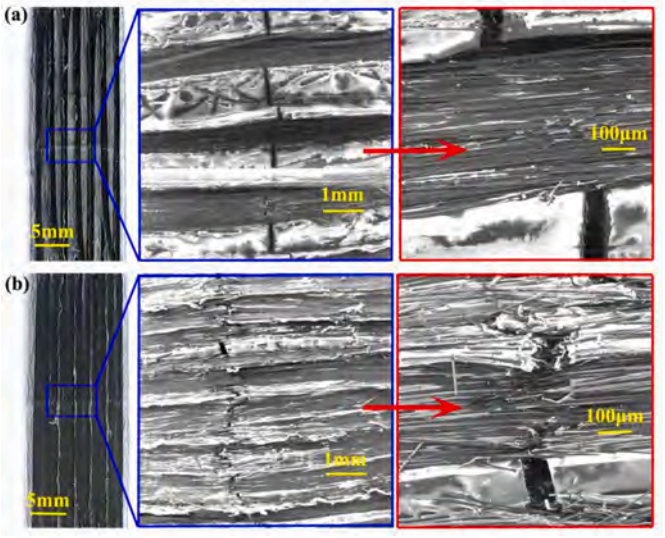

Fig. 10. Representative SEM images of the fracture surface after the three-point bending test of composite samples printed at the extrusion width of a) 1.9 mm and b) 0.9 mm.

The p-values of the models are evidently less than 0.05, which implies that the quadratic model selected in this study is significant. The values of R-squared are more than 96%, indicating a good agreement between the obtained prediction models and the existing experimental data. Moreover, the comparison of the predicted and experimental values of the bending response presented in Supplementary material section S2 also confirms the excellent agreement between the experimental data and the predicted ones.

The response surface plot presents the relationship between the mechanical response and any two model parameters in the form of a three-dimensional surface view, which assists in determining the desirable mechanical response value and the corresponding process conditions. Fig. 11 displays the three-dimensional surface diagrams of bending strength and flexural modulus of the 4D printed CFRSMPC specimens with various printing parameters, obtained depending on Eq. (5) and Eq. (6). In addition to determining the response under particular parameters by positional coordinates, the color gradient corresponding to the response level can also help to obtain a more intuitive response as a function of the two parameters. Besides, the solid lines on the response surface are contour lines representing the coupling relationship of two variables at the same response level.

As observed in Fig. 11a, the bending strength and flexural modulus of the specimens are positively correlated with the extruder temperature,

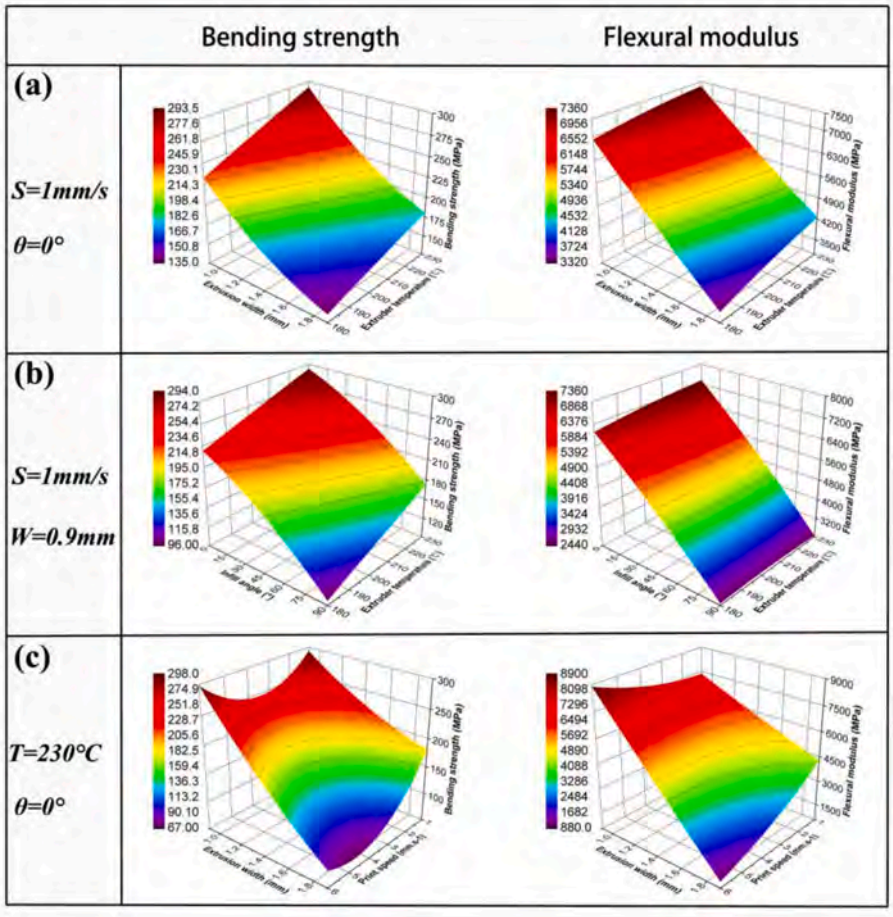

Fig. 11. 3D surface graphs of the relationship between printing parameters and bending properties including bending strength and flexural modulus. The graphs were presented when a) $S = 1$ mm/s and $\theta = 0°$, b) $S = 1$ mm/s and $W = 0.9$ mm, and c) $T = 230$ °C and $\theta = 0°$.

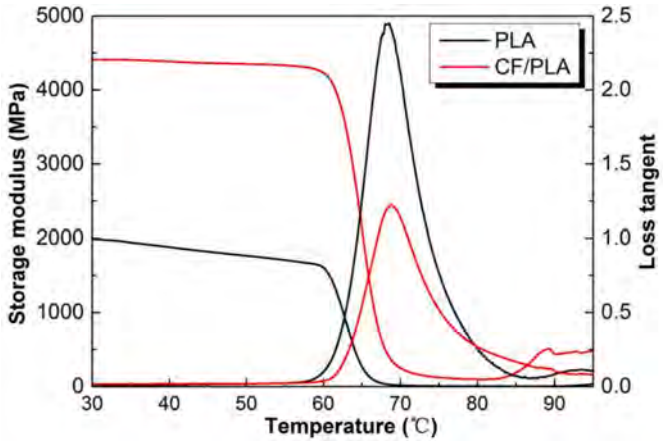

Fig. 12. Storage modulus and loss tangent of two kinds of printed materials.

and conversely, negatively correlated with the extrusion width. This is consistent with the results of previous experimental data analysis. The coupling effect of extruder temperature and extrusion width on bending performance showcases a diagonal law, that is, the bending strength and flexural modulus are the largest at the highest extruder temperature and the minimum extrusion width, while the values at the lowest extruder temperature and the maximum extrusion width are the smallest. A similar effect of the infill angle and the extruder temperature on the bending strength of the printed sample is presented in Fig. 11b. However, it is worth noting that the infill angle is the dominant factor in the coupling effect of infill angle and extruder temperature on flexural modulus, while the extruder temperature contributes little effect. The impact of printing speed on the bending properties of the printed sample varies with other parameters. As showed in Fig. 11c, when the extrusion width $W = 1.9$ mm, the bending strength of the sample increases as the printing speed decreases. However, when the extrusion width is about 0.9 mm, the bending strength of the sample decreases first and then increases as the printing speed decreases. In addition, it is observed from Fig. 11c that the flexural modulus exhibits more conspicuous change with the extrusion width at high printing speeds than at low printing speeds, which can be attributed to the impact of the prominently non-uniform temperature gradient at high printing speeds [38].

3.2. DMA results

The dynamic mechanical properties of printed pure PLA specimens and printed CFRSMPC specimens were measured by DMA. Dynamic storage modulus (E') and loss tangent (Tanδ) are analyzed in Fig. 12. It can be observed that the evolution curves of the storage modulus of the two samples can be divided into three stages including glass state, glass transition phase and rubber state, indicating that the storage modulus of pure PLA and CFRSMPC exhibits distinct variable stiffness characteristics with temperature. Perhaps the difference is that the storage modulus of printed CFRSMPC in the glass state is as high as 4408 MPa, which is 2.21 times of the storage modulus of printed pure PLA. This phenomenon proves that the addition of CFs not only does not affect the variable stiffness characteristics of the printed samples, but also dramatically improves their mechanical properties, which can expand the application

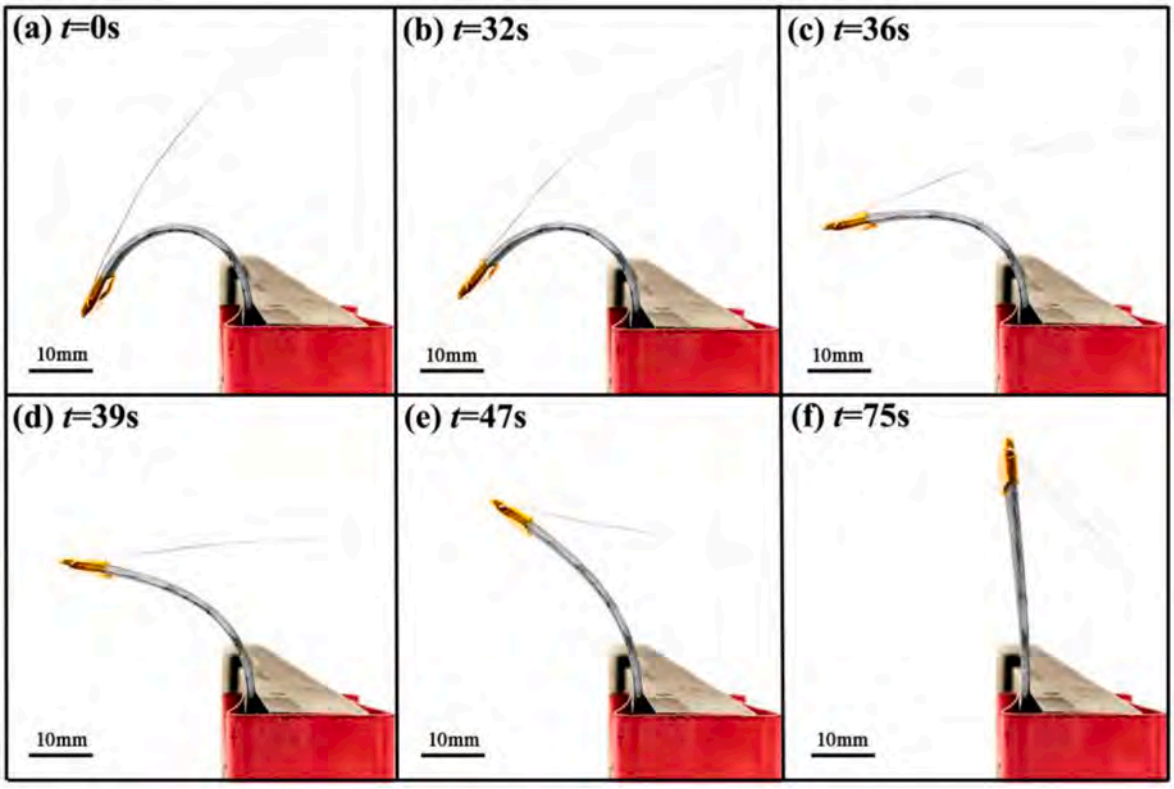

Fig. 13. Snapshot of Joule heating-induced shape recovery in 4D printed CFRSMPC.

prospect of 3D printing process.

The loss tangent is the ratio of the loss modulus to the storage modulus, which can reflect the viscosity characteristics of polymers. The incorporation of fibers will cause shear stress to form between the matrix and fibers, thereby reducing the additional power dissipation of the composite [39]. Therefore, as expected, it can be seen from Fig. 12 that the loss tangent of the printed CFRSMPC is significantly lower than the printed pure PLA. The temperature corresponding to the peak of the loss

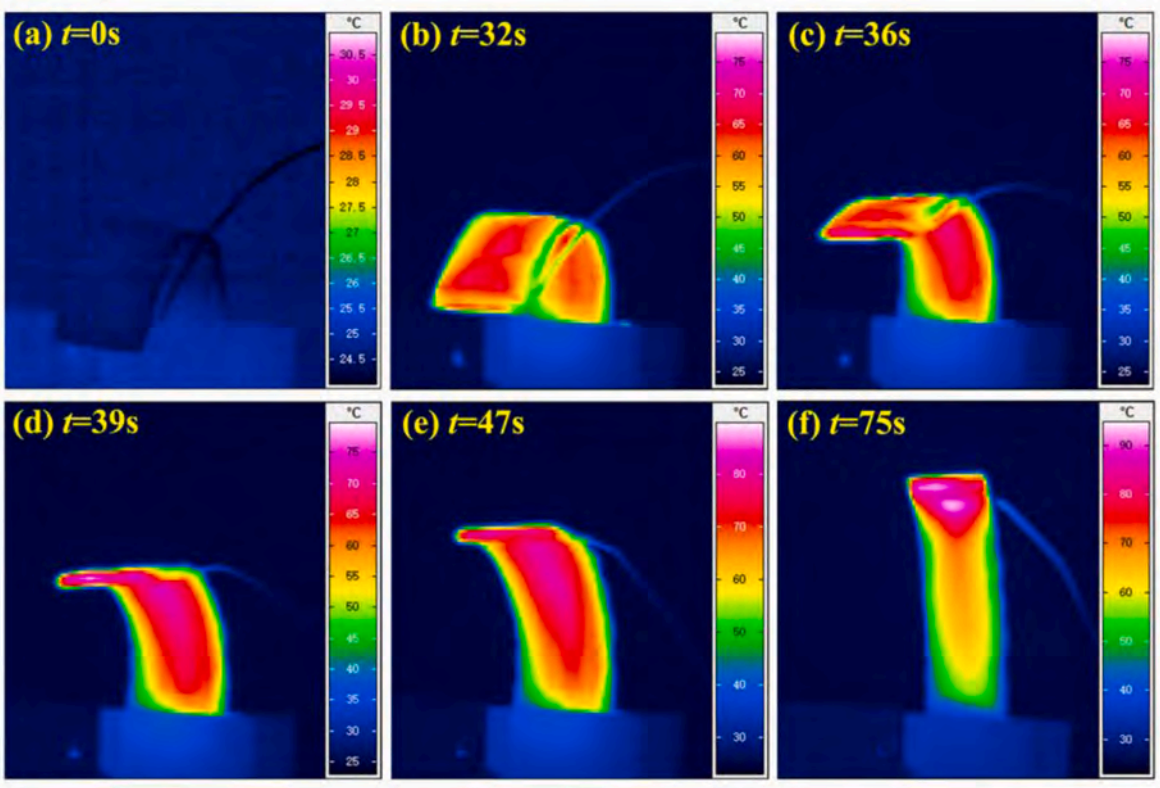

Fig. 14. Snapshots of shape recovery and temperature distribution of 4D printed CFRSMPC specimen during resistance heating.

tangent is defined as the T_g of the material. The molecular mobility of the thermoplastic PLA is significantly promoted at the T_g, and the material undergoes a phase transition from the glassy state to a rubbery state. It is observed that the T_g of the printed CFRSMPC is 69 °C, which is higher than the T_g (68 °C) of the printed pure PLA. The incorporation of fibers causes the T_g to shift to higher temperature, which is related to the reduced chain mobility by the added fibers [40].

3.3. Electro-induced shape memory behavior

3.3.1. Electrical actuation and shape recovery

4D printed CFRSMPC can be activated directly by temperature or by an electric circuit through the CF bundles, which indirectly causes the electrocaloric effect. The electro-induced shape memory effect of the printed CFRSMPC specimen was investigated in this study. In this process, shape change was achieved by performing resistance heating under ambient pressure conditions. The initial resistance of the v-shaped specimen was about 6Ω, and a voltage of 5 V was applied across the specimen until its shape no longer changed. Fig. 13 presents a visual description of the shape recovery of the 4D printed CFRSMPC sample. The entire recovery process lasts about 75 s, and the deformation of the sample occurs mainly within 30s and 50s. The apparent shape recovery process indicates that the 4D printed CFRSMPC possesses significant shape memory effect, which demonstrates that the resistance heating method is an effective way to drive the sample back to its initial shape.

Compared with other 4D printed materials [18], the employment of voltage instead of the direct temperature field to activate the shape recovery process is a major highlight of 4D printed CFRSMPC. Due to the high electrical conductivity and electrocaloric effect, the fiber bundles generate sufficient Joule heat at a specific voltage to raise the temperature of PLA-based SMP above its T_g, thereby inducing the phase transition of the polymer. An infrared thermal camera was employed to investigate the temperature distribution and temperature variation of 4D printed CFRSMPC specimens during the electric driving. At a rated voltage of 5 V, the temperature distribution in 4D printed CFRSMPC specimen along with the shape recovery process is presented in Fig. 14. According to the infrared thermal images, in addition to the low temperature region caused by the more easily occurring temperature dissipation at the edge portion, the temperature distribution in the specimen is relatively uniform, indicating that the electric resistance heating method is stable and feasible. The temperature in the specimen shows an upward trend as a whole with the energization time. The maximum temperature in the sample rises from RT to T_g of the material during the first 32 s, so the structure experiences quite small deformation. In this process, the Joule heat generated by CF bundles under the action of current diffuses into the matrix, causing the temperature of the matrix to rise continuously, but the temperature is not sufficient to stimulate the shape memory behavior of the shape memory polymer. Hence, the part hardly undergoes deformation. When the temperature in the matrix reaches its T_g, the shape memory effect of the matrix is stimulated, and the result is macroscopically expressed as rapid angular changes of the v-shaped specimen.

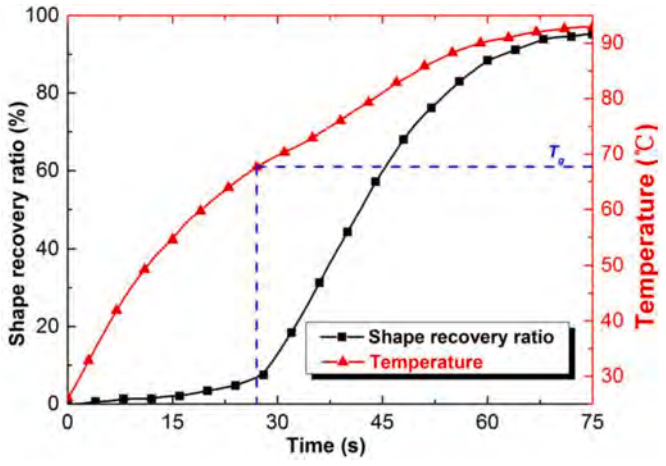

Fig. 15. Temperature changes and rotation angle α versus heating time during the shape recovery process for 4D printed CFRSMPC.

Fig. 15 presents the maximum temperature and shape recovery rate of the specimen as a function of the energization time. It should be mentioned that the average temperature in a specific area is difficult to determine, because the shape of the specimen changes during the heating process. Therefore, the evolution of the temperature with the energization time is investigated based on the maximum temperature in the specimen. The shape recovery rate can be defined by the following equation [41].

$$R_r = \frac{\alpha_0 - \alpha_n}{\alpha_0} \times 100\% \quad (7)$$

Where R_r is the shape recovery rate of the specimen, and α_0 and α_n are the initial angle and the real-time angle of the v-shaped sample defined according to Fig. 3b, respectively. The evolution curve of the shape recovery rate with the energization time can be divided into three stages. In the first stage, the shape recovery rate remains substantially unchanged, and the temperature increases dramatically. In the second stage, the temperature in the specimen reaches the T_g, and the shape recovery rate began to increase sharply. In the third stage, the shape recovery rate slowly increases until it remains stable, and the maximum temperature in the specimen tends to be stable due to heat dissipation. It can be seen from Fig. 15 that the maximum shape recovery rate of 4D printed CFRSMPC specimen is above 95%, indicating that the 4D printed CFRSMPC can serve as potential building blocks for electrically activated and deployable structures.

3.3.2. Deformation control through resistance measurement

During the shape memory test of the 4D printed CFRSMPC, changes in resistance at various bending angles and temperatures were observed. The quantitative influence of the bending angle and temperature on the resistance of the printed specimen was further investigated. The results demonstrate that real-time monitoring of the deformation of 4D printed CFRSMPC by means of resistance measurement is feasible. This methodology may be applied to future space deployable structures to control their deployment process. The experimental process simulated the typical thermo-mechanical cycle test method of SMP in four steps: heating, bending, cooling and recovery. The resistance value of the specimen during heating, bending and cooling was directly measured by a digital multimeter, while the resistance value of the specimen during the recovery process was obtained by Ohm's law based on the rated voltage and the measured current.

Fig. 16 shows how the resistance of the 4D printed CFRSMPC varied with relevant parameters at various stages of shape memory test. It can be observed from Fig. 16a that during the heating stage, the resistance of the specimen exhibits a positive temperature coefficient (PTC) effect. From room temperature to 90 °C, the resistance increases by 0.8 Ω from 3.1Ω to 3.9Ω. The PTC effect of carbon fiber reinforced thermoplastic composites has been reported [42,43]. The underlying reason for the PTC effect is the increase in the average spacing of the internal fibers [42]. The continuous CF bundle embedded in the PLA is comprised of micron-sized filaments with extremely small spacing from each other. The residual compressive strain derived from the rapid curing of PLA during the 4D printing process causes the CF to be pushed together. During the heating process, the release of residual strain and the rebound of CFs reduce the number of inter-fiber contacts, which results in an increase in resistance.

Fig. 16b depicts the variation of resistance with the bending angle during the specimen bending process at a temperature of about 90 °C.

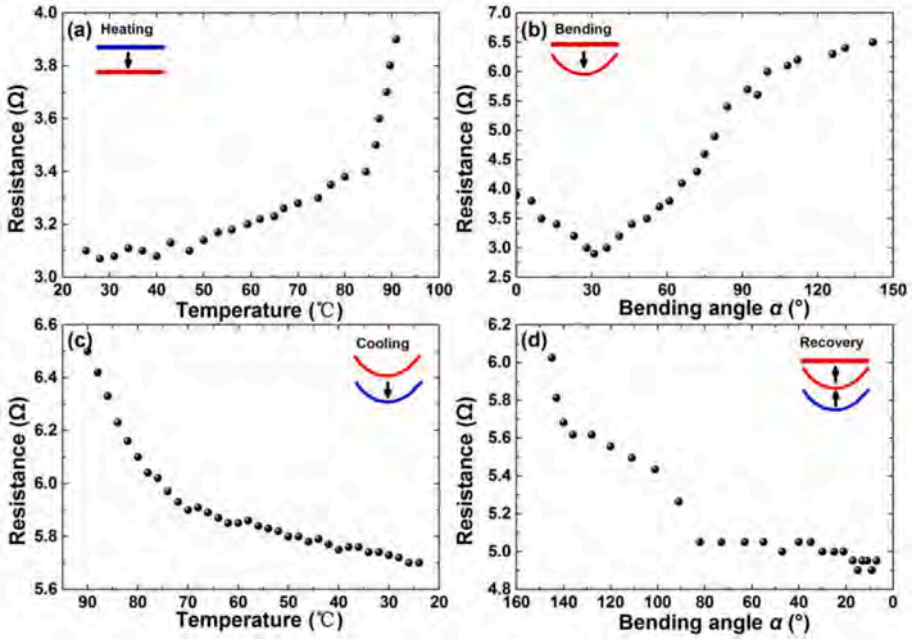

Fig. 16. The resistance of 4D printed CFRSMPC specimen changes with the relevant parameters during the shape memory test. a) Resistance versus temperature during the heating stage. b) Resistance versus bending angle α during the bending stage. c) Resistance versus temperature during the cooling stage. d) Resistance versus bending angle α during the recovery stage.

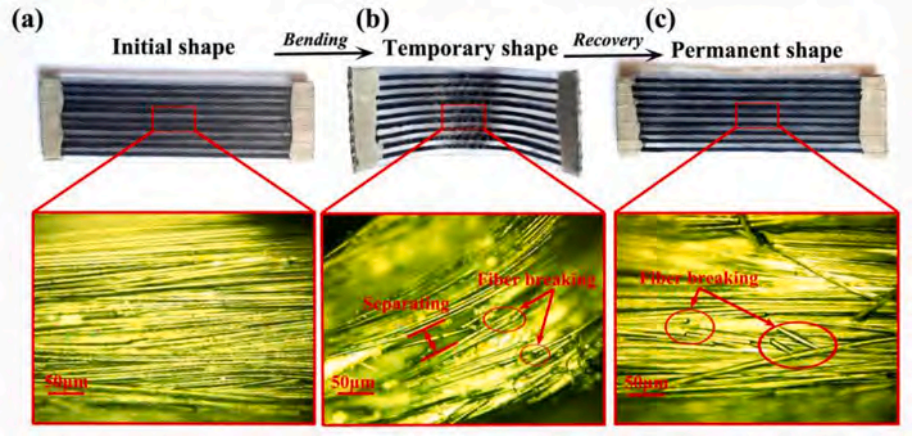

Fig. 17. The macrostructure of 4D printed CFRSMPC specimens in the shape memory test process and the microscopic morphology of the carbon fiber observed with an optical microscope. a) Specimen with the rectangular initial shape before bending. b) Specimen with V-shaped temporary shape in which obvious fiber buckling deformation occurred after bending. c) Specimen with permanent shape after recovery.

During the change from the initial shape to the temporary shape, the resistance of the specimen performs decreasing previously and increasing later obviously. The initial decrease in the resistance results from the increased inter-fiber contacts caused by fiber tension under large curvature bending. The subsequent increase in the resistance is mainly attributed to fiber buckling and breakage induced by further bending. Fig. 17a and b present the macroscopic and microscopic morphology of the specimens before and after bending. Before bending, the surface of the specimen is flat and the fiber bundles are tightly arranged, indicating that the specimen has good electrical conductivity. However, when the specimen is bent into a v-shaped temporary shape, wrinkles occur in the main deformation region of the specimen, demonstrating significant fiber bending and fiber buckling [44]. As shown in the optical micrograph in Fig. 17b, the filaments are separated from each other as well as fibers breakage occurs as a result of the unsynchronized buckling behavior of the filaments in fiber bundles, which reduces inter-fiber contacts, resulting in increased electrical resistance of specimen. In addition, it is generally believed that a CF microstructure primarily consists of layers of long sheets of sp2-bonded carbon atoms (graphite layers) [45]. In the direction perpendicular to the graphite layer, the macro-buckling of the fibers may lead to an increase in the spacing of graphite layers. As a result, the density-of-state of the π electrons decreases, and higher resistance is measured as electrons are forced to move a greater distance from one graphite layer to another.

The phenomenon of the decrease in the resistance of 4D printed CFRSMPC during the cooling process observed in Fig. 16c is caused by the reverse process of the PTC effect. In fact, the matrix around the fibers shrinks during cooling, reducing the spacing of the filaments from each other and increasing the number of inter-fiber contacts. Fig. 16d exhibits the resistance measurement of the specimen during electrical heating recovery. In the initial stage of deformation, the resistance decreases dramatically by 5.6% from 6.02Ω to 5.68Ω. This dramatic reduction can be attributed to the instantaneous start-up of the shape recovery process. When the temperature in the specimen rises to its T_g under the action of

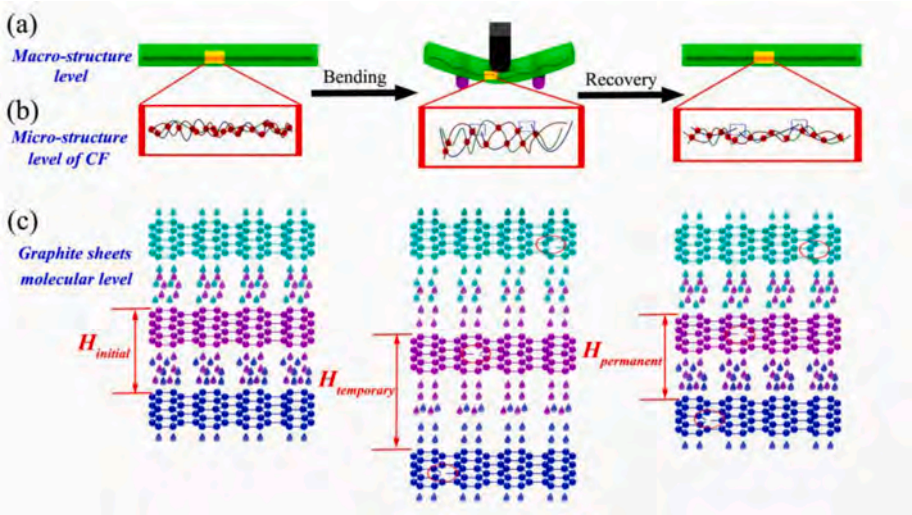

Fig. 18. The phenomenological model, which demonstrates the mechanism of resistance change during bending and recovery of 4D printed CFRSMPC from three levels: (a) macro-structure level, (b) micro-structure level of CF and (c) graphite sheets molecular level.

Joule heat, the shape memory effect of the material is instantaneously stimulated, and the residual stress and buckling deformation stored during the bending process are released in a relatively short period of time, resulting in smaller graphite layer spacing and higher density of π electrons and thus, lower resistivity. A clear comparison of the macro and micro morphologies of the specimens before and after the recovery in Figs. 17b and c can be served as proof of this interpretation.

Based on the previous analysis of the change in the resistance of 4D printed CFRSMPC during the shape memory test, a phenomenological model presented in Fig. 18 is proposed to support the deformation monitoring and control of the printed composite structures. The model demonstrates the mechanism of the resistance change of 4D printed CFRSMPC from three hierarchies: macro-structure of a printed specimen, micro-structure of CFs and molecular structure of graphite layers. The macro-structure showed in Fig. 18a depicts two processes in which the specimen is bent from the initial shape to the v-shaped temporary shape and then returned to the permanent shape, which are respectively associated with the occurrence and release of buckling deformation. Fig. 18b shows the internal contact of the filaments in the specimen. The red circles represent electrical contact points that can cause excellent electrical conductivity. The CF filaments in the temporary shape are separated from each other due to the buckling effect, resulting in less electrical contact points and, therefore, large electrical resistance. The blue rectangular frame encircles the region where fiber breakage occurs, which also results in higher resistivity. The molecular structure of the graphite layers exhibited in Fig. 18c describes the change in the graphite molecular layers spacing and the density-of-state of the π electrons when the macroscopic buckling of CFs occurs. The spheres represent carbon atoms, the straight lines between each carbon atom represent carbon-carbon covalent bonds, and the water droplet symbols among the graphite layers represent π electrons that can be freely exchanged between graphite layers. As the specimen is bent from its initial shape to a v-shaped temporary shape, the graphite molecular layers spacing becomes larger ($H_{initial} < H_{temporary}$) and the density of the π electrons which can freely move between the layers is lowered, which results in a larger resistivity of the material. When the specimen is returned from the temporary shape to the permanent shape, graphite molecular layers spacing becomes smaller ($H_{temporary} > H_{permanent}$) and the density-of-state of the π electrons increases, causing the resistivity to decrease. In addition, when an external load is applied, the carbon-carbon covalent bonds in the graphite layers may break, which also leads to a decrease in the electrical conductivity of the material.

4. Summary and conclusions

A 3D printer based on FDM with dual feed channels was modified to fabricate CFRSMPC with diverse fiber laying directions and fiber volume fractions. The three-point bending tests were carried out to evaluate the effect of various printing parameters on the bending strength and flexural modulus of 4D printed CFRSMPC. The results show that higher extruder temperatures promote impregnation of the molten thermoplastic matrix with continuous CFs, resulting in higher bending performance and lower surface roughness of the printed components. However, higher printing speed causes weak interface bonding, implying poor mechanical response. In addition, the mathematical prediction models based on existing experimental data were established to describe the coupling effect of printing parameters on the bending properties of 4D printed CFRSMPC. The DMA and electric heating shape recovery tests were used to characterize the variable stiffness characteristic and electro-induced shape memory effect of 4D printed CFRSMPC, respectively. CF bundles as the resistance heating elements generated Joule heat at a specific voltage to provide sufficient thermal stimulus for the shape recovery process of the CFRSMPC. At a voltage of 5 V, the deployment process of the CFRSMPC specimen was performed during 75 s and the shape recovery rate was higher than 95%. Finally, the quantitative influence of bending angle and temperature on the resistance of 4D printed CFRSMPC during the programming and recovery process was further studied, and a phenomenological model was established to demonstrate the mechanism of the resistance change of 4D printed CFRSMPC specimen during the bending and recovery process. The results demonstrate that it is possible to monitor the real-time deformation of 4D printed CFRSMPC through the resistance measurement method. This approach is expected to be applied to future space deployable structures to control their deployment process.

In conclusion, the continuous carbon fiber reinforced shape memory polymer composite fabricated by 4D printing not only overcomes the shortcomings of the traditional 3D printed structures that cannot achieve active deformation, but also greatly improves the mechanical strength compared with common 3D printed pure polymer or particle reinforced composite structure [46,47], which can serve as key elements for electrically heated and deployable structures. 4D printing technology of continuous carbon fiber reinforced shape memory polymer composite is a novel manufacturing technology, and further work is needed to develop complex components to enhance the application prospect of this technology.

Declaration of competing interest

The authors declare that they have no known competing financial interests or personal relationships that could have appeared to influence the work reported in this paper.

CRediT authorship contribution statement

Chengjun Zeng: Conceptualization, Investigation, Visualization, Writing - original draft, Writing - review & editing. **Liwu Liu:** Conceptualization, Methodology, Supervision, Data curation, Writing - review & editing. **Wenfeng Bian:** Visualization, Investigation, Data curation, Writing - review & editing. **Yanju Liu:** Visualization, Investigation, Writing - review & editing. **Jinsong Leng:** Conceptualization, Methodology, Investigation, Writing - review & editing.

Acknowledgements

This work was supported by the National Natural Science Foundation of China (Grant Nos. 11632005 and 11672086).

Appendix A. Supplementary data

Supplementary data to this article can be found online at https://doi.org/10.1016/j.compositesb.2020.108034.

References

[1] Yang H, Leow WR, Wang T, Wang J, Yu J, He K, Qi D, Wan C, Chen X. 3D printed photoresponsive devices based on shape memory composites. Adv Mater 2017;29:1701627.
[2] Wang J, Li H, Liu R, Li L, Lin Y, Nan C. Thermoelectric and mechanical properties of PLA/Bi 0·5 Sb 1·5 Te 3 composite wires used for 3D printing. Compos Sci Technol 2018;157:1–9.
[3] Gonzalez-Henriquez CM, Sarabia-Vallejos MA, Rodriguez-Hernandez J. Polymers for additive manufacturing and 4D-printing: materials, methodologies, and biomedical applications. Prog Polym Sci 2019;94:57–116.
[4] Akbari S, Sakhaei AH, Kowsari K, Yang B, Serjouei A, Zhang Y, et al. Enhanced multimaterial 4D printing with active hinges. Smart Mater Struct 2018;27(6):065027.
[5] Lui Y, Sow W, Tan L, Wu Y, Lai Y, Li H. 4D printing and stimuli-responsive materials in biomedical applications. Acta Biomater 2019;92:19–36.
[6] Tibbits S. 4D printing: multi-material shape change. Architect Des 2014;84(1):116–21.
[7] Bodaghi M, Damanpack A, Liao W. Adaptive metamaterials by functionally graded 4D printing. Mater Des 2017;135:26–36.
[8] Zhao W, Zhang F, Leng J, Liu Y. Personalized 4D printing of bioinspired tracheal scaffold concept based on magnetic stimulated shape memory composites. Compos Sci Technol 2019;184:107866.
[9] Guo J, Zhang R, Zhang L, Cao X. 4D printing of robust hydrogels consisted of agarose nanofibers and polyacrylamide. ACS Macro Lett 2018;7:442–6.
[10] Wang W, Yu CY, Serrano PAA, Ahn SH. Soft grasping mechanisms composed of shape memory polymer based self-bending units. Compos B Eng 2019;164:198–204.
[11] Zhang W, Zhang F, Lan X, Leng J, Wu AS, Bryson TM. Shape memory behavior and recovery force of 4D printed textile functional composites. Compos Sci Technol 2018;160:224–30.
[12] Mu T, Liu L, Lan X, Liu Y, Leng J. Shape memory polymers for composites. Compos Sci Technol 2018;160:169–98.
[13] Invernizzi M, Turri S, Levi M, Suriano R. 4D printed thermally activated self-healing and shape memory polycaprolactone-based polymers. Eur Polym J 2018;101:169–76.
[14] Michal BT, Spencer EJ, Rowan SJ. Stimuli-responsive reversible two-level adhesion from a structurally dynamic shape-memory polymer. ACS Appl Mater Interfaces 2016;8(17):11041–9.
[15] Herath HMCM, Epaarachchi JA, Islam MM, Al-Azzawi W, Leng J, Zhang F. Structural performance and photothermal recovery of carbon fibre reinforced shape memory polymer. Compos Sci Technol 2018;167:206–14.
[16] Xu Z, Ding C, Wei D, Bao R, Ke K, Liu Z, et al. Electro and light-active actuators based on reversible shape-memory polymer composites with segregated conductive networks. ACS Appl Mater Interfaces 2019;11(33):30332–40. 2019.
[17] Ze Q, Kuang X, Wu S, Wong J, Montgomery SM, Zhang R, Kovitz JM, Yang F, Qi HJ, Zhao R. Magnetic shape memory polymers with integrated multifunctional shape manipulation. Adv Mater 2019;32(4):1906657.
[18] Liu Y, Zhang F, Leng J, Wang L, Cotton C, Sun B, Chou TW. Synergistic effect enhanced shape recovery behavior of metal-4D printed shape memory polymer hybrid composites. Compos B Eng 2019;179:107536.
[19] Liu Y, Zhang W, Zhang F, Leng J, Pei S, Wang L, et al. Microstructural design for enhanced shape memory behavior of 4D printed composites based on carbon nanotube/polylactic acid filament. Compos Sci Technol 2019;181:107692.
[20] Rosales CAG, Duarte MFG, Kim H, Chave L, Hodges D, Mandal P, et al. 3D printing of shape memory polymer (SMP)/carbon black (CB) nanocomposites with electro-responsive toughness enhancement. Mater Res Express 2018;5(6):065704.
[21] Zhao W, Zhang F, Leng J, Liu Y. Personalized 4D printing of bioinspired tracheal scaffold concept based on magnetic stimulated shape memory composites. Compos Sci Technol 2019;184:107866.
[22] Lin C, Lv J, Li Y, Zhang F, Li J, Liu Y, Liu L, Leng J. 4D-Printed biodegradable and remotely controllable shape memory occlusion devices. Adv Funct Mater 2019;29(51):1906569.
[23] Ferreira RTL, Amatte IC, Dutra TA, Bürger D. Experimental characterization and micrography of 3D printed PLA and PLA reinforced with short carbon fibers. Compos B Eng 2017;124:88–100.
[24] Liu T, Tian X, Zhang M, Abliz D, Li D, Ziegmann G. Interfacial performance and fracture patterns of 3D printed continuous carbon fiber with sizing reinforced PA6 composites. Compos Appl Sci Manuf 2018;114:368–76.
[25] Li N, Li Y, Liu S. Rapid prototyping of continuous carbon fiber reinforced polylactic acid composites by 3D printing. J Mater Process Technol 2016;238:218–25.
[26] Heidari-Rarani M, Rafiee-Afarani M, Zahedi AM. Mechanical characterization of FDM 3D printing of continuous carbon fiber reinforced PLA composites. Compos B Eng 2019;175:107147.
[27] Chacón JM, Caminero MA, Núñez PJ, García-Plaza E, García-Moreno I, Reverte JM. Additive manufacturing of continuous fibre reinforced thermoplastic composites using fused deposition modelling: effect of process parameters on mechanical properties. Compos Sci Technol 2019;181:107688.
[28] Sugiyama K, Matsuzaki R, Ueda M, Todoroki A, Hirano Y. 3D printing of composite sandwich structures using continuous carbon fiber and fiber tension. Compos Appl Sci Manuf 2018;113:114–21.
[29] Liu T, Liu L, Zeng C, Liu Y, Leng J. 4D printed anisotropic structures with tailored mechanical behaviors and shape memory effects. Compos Sci Technol 2020;186:107935.
[30] Caminero MA, Chacón JM, Garcia-Moreno I, Rodriguez GP. Impact damage resistance of 3D printed continuous fibre reinforced thermoplastic composites using fused deposition modelling. Compos B Eng 2018;148:93–103.
[31] Ding Q, Li X, Zhang D, Zhao G, Sun Z. Anisotropy of poly (lactic acid)/carbon fiber composites prepared by fused deposition modeling. J Appl Polym Sci 2019:48786.
[32] Kuznetsov VE, Solonin AN, Tavitov A, Urzhumtsev O, Vakulik A. Increasing strength of FFF three-dimensional printed parts by influencing on temperature-related parameters of the process. Rapid Prototyp J 2020;26(1):107–21.
[33] Jaekel DJ, MacDonald DW, Kurtz SM. Characterization of PEEK biomaterials using the small punch test. J Mech Behav Biomed Mater 2011;4:1275–82.
[34] Wang P, Zou B, Xiao H, Ding S, Huang C. Effects of printing parameters of fused deposition modeling on mechanical properties, surface quality, and microstructure of PEEK. J Mater Process Technol 2019;271:62–74.
[35] Tian X, Liu T, Yang C, Wang Q, Li D. Interface and performance of 3D printed continuous carbon fiber reinforce of PLA composites. Compos Appl Sci Manuf 2016;88:198–205.
[36] Huang B, Meng S, He H, Jia Y, Xu Y, Huang H. Study of processing parameters in fused deposition modeling based on mechanical properties of acrylonitrile-butadiene-styrene filament. Polym Eng Sci 2019;59(1):120–8.
[37] Hu Q, Duan Y, Zhang H, Liu D, Yan B, Peng F. Manufacturing and 3D printing of continuous carbon fiber prepreg filament. J Mater Sci Composites 2018;53(3):1887–98.
[38] Luzanin O, Guduric V, Ristic I, Muhic S. Investigating impact of five build parameters on the maximum flexural force in FDM specimens–a definitive screening design approach. Rapid Prototyp J 2017;23(6):1088–98.
[39] Cordeiro EP, Pita VJ, Soares BG. Epoxy–fiber of peach palm trees composites: the effect of composition and fiber modification on mechanical and dynamic mechanical properties. J Polym Environ 2017;25(3):913–24.
[40] Pothan LA, Oommen Z, Thomas S. Dynamic mechanical analysis of banana fiber reinforced polyester composites. Compos Sci Technol 2003;63(2):283–93.
[41] Li M, Wu J, Song F, Li D, Wang X, Chen L, et al. Flexible and electro-induced shape memory Poly(Lactic Acid)-based material constructed by inserting a main-chain liquid crystalline and selective localization of carbon nanotubes. Compos Sci Technol 2019;173:1–6.
[42] Zhang R, Tang P, Li J, Xu D, Bin Y. Study on filler content dependence of the onset of positive temperature coefficient (PTC) effect of electrical resistivity for UHMWPE/LDPE/CF composites based on their DC and AC electrical behaviors. Polymer 2014;55(8):2103–12.
[43] Zhang X, Zheng X, Ren D, Liu Z, Yang W, Yang M. Unusual positive temperature coefficient effect of polyolefin/carbon fiber conductive composites. Mater Lett 2016;164:587–90.
[44] Lan X, Liu L, Liu Y, Leng J. Post microbuckling mechanics of fibre-reinforced shape-memory polymers undergoing flexure deformation. Mech Mater 2014;72:46–60.
[45] Joshi K, Arefev MI, Zhigilei LV. Generation and characterization of carbon fiber microstructures by atomistic simulations. Carbon 2019;152:396–408.
[46] Liu H, He H, Peng X, Huang B, Li J. Three-dimensional printing of poly (lactic acid) bio-based composites with sugarcane bagasse fiber: effect of printing orientation on tensile performance. Polym Adv Technol 2019;30(4):910–22.
[47] Wu W, Jiang J, Jiang H, Liu W, Li G, Wang B, et al. Improving bending and dynamic mechanics performance of 3D printing through ultrasonic strengthening. Mater Lett 2018;220:317–20.